Applied Mathematical Modelling 76 (2019) 545–557

Contents lists available at ScienceDirect

Applied Mathematical Modelling

journal homepage: www.elsevier.com/locate/apm

Torsional stick-slip vibrations and multistability in drill-strings

Yang Liu[a,*], Wei Lin[a,b], Joseph Páez Chávez[c,d], Rulston De Sa[e]

[a] College of Engineering, Mathematics and Physical Sciences, University of Exeter, North Park Road, Exeter EX4 4QF, UK
[b] School of Mechatronic Engineering, Southwest Petroleum University, Chengdu 610500, China
[c] Center for Applied Dynamical Systems and Computational Methods (CADSCOM), Faculty of Natural Sciences and Mathematics, Escuela Superior Politécnica del Litoral, P.O. Box 09-01-5863, Guayaquil, Ecuador
[d] Center for Dynamics, Department of Mathematics, TU Dresden, Dresden D-01062, Germany
[e] 2H Offshore Engineering Ltd., Tern Place House, Tern Place, Bridge of Don, Aberdeen AB23 8JX, UK

ARTICLE INFO

Article history:
Received 26 October 2018
Revised 29 May 2019
Accepted 12 June 2019
Available online 18 June 2019

Keywords:
Drill-string
Stick-slip
Multistability
Nonsmooth dynamical system
Numerical continuation

ABSTRACT

The generalized lumped-parameter model of the drill-string system is studied in this paper to provide a fundamental understanding of the torsional stick-slip vibrations in downhole drilling. Our investigation focuses on analysing the cause of three coexisting states: bit sticking, stick-slip vibration, and constant rotation. A critical region of multistability is identified based on the lumped-parameter model, and the conditions for switching between these multiple stable states are discussed. Special attention is given to the bifurcation structure of the considered drill-string model, which is obtained via path-following methods for nonsmooth dynamical systems. The bifurcation scenario is compared to the case when a longer drill-string is considered, which amounts to drilling deeper. It is found that the main features of the bifurcation picture persist under variation of the drill-string length, with certain numerical differences regarding for instance the window of multistability.

1. Introduction

The oil and gas energy sector provides non-renewable natural resources which have become crucial to everyday life. The acquisition of these hydrocarbons is predominantly dependent on oil companies utilising the drilling process, and on average, drilling operations account for approximately 40% of all expenses involved in the exploration and production [1]. Therefore, it is highly desirable for these companies to keep this figure to a minimum, given the vast amount of investments currently presiding in the oil and gas sector. To accomplish this, the equipment involved in drilling processes, for instance oil well drill-strings as shown in Fig. 1(a), should be optimised to keep operation costs and times low, while achieving high rates of penetration. Along these lines, harmful vibrations, such as stick-slip, bit bounce and whirling (see Fig. 1(b)) have been identified as the main causes for high operation costs and significantly low penetration rates. Since these phenomena can lead to catastrophic failures of the drilling rig, or at the very least degradation of the expensive components involved in the drill-string, optimisation methods should be developed with the main motive of suppressing these phenomena, and

* Corresponding author.
E-mail addresses: y.liu2@exeter.ac.uk (Y. Liu), weilin_swpu@hotmail.com (W. Lin), jpaez@espol.edu.ec (J. Páez Chávez), Rulston.DeSa@2hoffshore.com (R. De Sa).

https://doi.org/10.1016/j.apm.2019.06.012

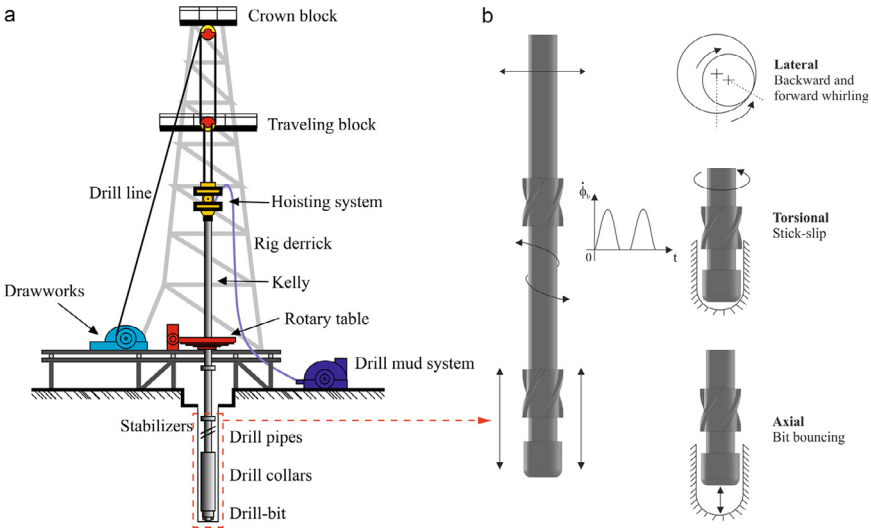

Fig. 1. (Colour online) Schematics of (a) an oilwell drilling rig [7] and (b) lateral, torsional and axial vibrations encountered in drill-strings during operation, where $\dot{\phi}_b$ is the angular velocity of the drill-bit and t is the time.

as a result, keeping drilling expenses low. This problem has attracted much attention in the past years, see e.g. [2–11]. The present work will study the torsional stick-slip vibrations of drill-strings using a generalized lumped-parameter model [9], focusing on the presence of multistability, with special attention given to the coexistence of stable states related to stick-slip, constant rotation and bit sticking. These types of responses are typically observed in real applications and one of our main goals is to propose control strategies to avoid undesirable vibrations, such as stick-slip. For this reason, coupled axial-torsional motions of the drill-strings associated with state-dependent delay, e.g. [12–15], which may bring extra dynamics to the drill-strings, will not be considered in this work.

In order to develop control and optimisation strategies for drill-strings, a great deal of theoretical and experimental research surrounding drill-string dynamics have been carried out in the past years [4]. From the results reported in [16–19], it has been determined that the main cause for stick-slip phenomena are the frictional forces acting on the drill-bit at the bit-rock interface. Furthermore, according to [16], the negative damping in the frictional forces due to the bit-rock interactions could be one of the causes of these harmful vibrations. Leine et al. [20] proposed a three degrees-of-freedom drill-string model which can observe stick-slip and whirl vibrations simultaneously. Melakhessou et al. [21] studied the local contact and the friction between the drill-string and casing, as well as the compressed bottom-hole-assembly in order to understand the complex behaviour of the drill-string system. In [22], reduced-order models of a drill-string system, which allow for radial, bending and torsion motions of a flexible drill-string and stick-slip interactions between the drill-string and the outer shell, were developed. Qualitative changes in system motion were studied numerically and experimentally with respect to rotation speed and the friction coefficient between the drill-string and the outer shell. In order to gain a deeper insight into the root cause of these vibrations, Kapitaniak et al. [7] developed an experimental drilling rig which was used to mimic all major drill-string vibrations. The nonlinear characteristics of the drill-string were then modelled using finite element methods and verified through experiments.

In the work by Dunayevsky and Abbassian [23], the authors studied the influence of using various drill-strings on the stability of the drilling operation, in regards to undesired torsional vibrations. Additional parametric studies were carried out by Kamel and Yigit [24], who investigated the effects of varying operational drilling parameters. In their work, the main conclusion was that when the axial feed rate during operation is increased, the rate of penetration and the applied weight-on-bit (WOB) are also increased, which nevertheless results in axial and torsional stick-slip vibrations. Therefore, this study suggests that lowering the WOB and the torque on bit could be used as control methods for suppressing stick-slip. Another relevant observation in this work was that the stick-slip vibrations can be reduced by suitably modifying the speed of the rotary table. A similar conclusion was obtained by Tang et al. [25], where the effects of the speed of rotary table on stick-slip were investigated. It was found that increasing the rotary table speed had effects on the period of the stick phase in stick-slip vibrations. Navarro-López and coworkers [1,3] confirmed this effect, who in addition investigated the effect of varying the control torque on the rotary table and the applied WOB on the stick-slip vibrations.

Another issue that has been analysed in the past concerns parameter uncertainty in drilling applications. In [26], Liu et al. proposed the utilisation of a Kalman estimator to deal with unmeasured downhole parameters. The numerical simulations showed that the proposed estimator was capable of identifying stick-slip vibrations and estimating downhole friction torque, thus leading to a decrease in the occurrence of stick-slip. Liu [27] proposed a sliding-mode control method to suppress stick-slip vibrations, assuming that the physical parameters of the drill-string were unknown. A robust output-feedback control to eliminate stick-slip in a drill-string system was presented in [28]. The control system proved to have major advantages

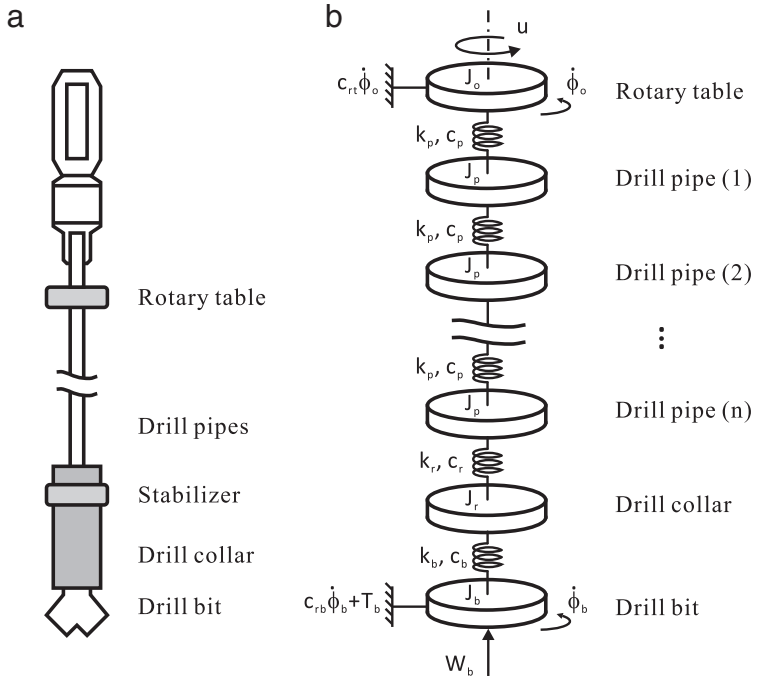

Fig. 2. (a) Schematics of a drill-string and (b) the lumped-parameter model of the drill-string system [27].

as it only requires surface measurements for operation. It can also effectively deal with unknown parameters regarding the bit-rock interactions and deal with multiple torsional flexibility modes.

The present work considers the lumped-parameter model of a drill-string that is capable of accounting for a variable length, by taking or adding rotating disks, which mimics the action of changing the number of drill pipes during operation. Our investigation concentrates on the torsional vibrations of the drill-string, and special attention is given to the multistability of the model, where coexisting attractors are found. For this study, specialized numerical techniques based on numerical continuation methods for nonsmooth dynamical systems, implemented via the computational platform COCO [29], are used. The drill-string model considered in the present work has followed closely the physical setting proposed and analyzed by Navarro-López [1,3,30,31]. Her analysis has primarily focused on the study of friction-induced stick-slip vibrations, based on a simplified torsional lumped-parameter model of an oilwell drill-string with multiple degrees of freedom. The starting point is a system response with constant bit rotation, corresponding to an equilibrium solution of the system after a suitable coordinate transformation. As, for example, the WOB increases, such equilibrium solution can be destabilized via a Hopf bifurcation, after which torsional vibrations in the drill-string take place. These vibrations can increase in amplitude, in such a way that at some point the drill-bit velocity can become zero. At this point, a grazing-sliding bifurcation takes place, after which stick-slip phenomena can be observed. Up to this point Navarro-López's work has provided great insight, both via analytical methods and numerical techniques based on path-following methods for smooth dynamical systems. A deeper understanding of the observed stick-slip vibrations can be achieved via the application of path-following techniques for nonsmooth dynamical systems, as this allows us to carry out the numerical continuation of stick-slip solutions, a task that cannot be performed via standard continuation methods. In this way, we are able to classify the system dynamics in detail, when varying two main control parameters, that is, the control torque and the WOB. This classification is based on the detection of discontinuity-induced bifurcations, such as grazing-sliding and boundary-equilibrium bifurcation, in connection to classical bifurcations (Hopf bifurcation of equilibria and fold bifurcation of limit cycles).

The rest of the paper is organized as follows. In Section 2, the lumped-parameter model of the drill-string system is introduced and discussed. The mathematical formulation of the drill-string system in COCO is studied in Section 3. A detailed bifurcation analysis of the system is carried out in Section 4 by considering the conditions for multistability, the variations of WOB, drill-string length, and control torque. Finally, the paper finishes with some concluding remarks, given in Section 5.

2. Mathematical modelling of torsional motion of the drill-strings

2.1. Mathematical modelling

The generalized lumped-parameter model shown in Fig. 2 can be written in a single-input and multi-output form as follows

$$J\ddot{\Phi} + C\dot{\Phi} + K\Phi + T = U, \tag{1}$$

where $\Phi(t) = [\phi_o, \phi_1, \phi_2, \ldots, \phi_n, \phi_r, \phi_b]^T \in \mathbb{R}^{n+3}$ is a vector containing the angular positions of the discs, t is the time, $J = \text{diag}(J_o, \underbrace{J_p, J_p, \ldots, J_p}_{n}, J_r, J_b) \in \mathbb{R}^{(n+3)\times(n+3)}$ is the inertia matrix, $C \in \mathbb{R}^{(n+3)\times(n+3)}$ is the torsional damping matrix given by

$$C = \begin{bmatrix} c_p + c_{rt} & -c_p & 0 & 0 & \ldots & 0 & 0 & 0 & 0 \\ -c_p & 2c_p & -c_p & 0 & \ldots & 0 & 0 & 0 & 0 \\ 0 & -c_p & 2c_p & -c_p & \ldots & 0 & 0 & 0 & 0 \\ \ldots & \ldots & \ldots & \ldots & \ldots & \ldots & \ldots & \ldots & \ldots \\ 0 & 0 & 0 & 0 & \ldots & -c_p & c_p + c_r & -c_r & 0 \\ 0 & 0 & 0 & 0 & \ldots & 0 & -c_r & c_r + c_b & -c_b \\ 0 & 0 & 0 & 0 & \ldots & 0 & 0 & -c_b & c_b + c_{rb} \end{bmatrix},$$

$K \in \mathbb{R}^{(n+3)\times(n+3)}$ is the torsional stiffness matrix given by

$$K = \begin{bmatrix} k_p & -k_p & 0 & 0 & \ldots & 0 & 0 & 0 & 0 \\ -k_p & 2k_p & -k_p & 0 & \ldots & 0 & 0 & 0 & 0 \\ 0 & -k_p & 2k_p & -k_p & \ldots & 0 & 0 & 0 & 0 \\ \ldots & \ldots & \ldots & \ldots & \ldots & \ldots & \ldots & \ldots & \ldots \\ 0 & 0 & 0 & 0 & \ldots & -k_p & k_p + k_r & -k_r & 0 \\ 0 & 0 & 0 & 0 & \ldots & 0 & -k_r & k_r + k_b & -k_b \\ 0 & 0 & 0 & 0 & \ldots & 0 & 0 & -k_b & k_b \end{bmatrix},$$

$T = [0, 0, \ldots, T_b]^T \in \mathbb{R}^{n+3}$, and $U = [u, 0, \ldots, 0]^T \in \mathbb{R}^{n+3}$, where u is the control torque input. Furthermore, T_b is the torque of friction when the drill-bit contacts with the rock given by

$$T_b = \begin{cases} \tau_r & \text{if } |\dot{\phi}_b| < \xi \text{ and } |\tau_r| \le \tau_s, \\ \tau_s \text{sgn}(\tau_r) & \text{if } |\dot{\phi}_b| < \xi \text{ and } |\tau_r| > \tau_s, \\ \mu_b R_b W_b \, \text{sgn}(\dot{\phi}_b) & \text{if } |\dot{\phi}_b| \ge \xi, \end{cases} \tag{2}$$

where τ_r is the reaction torque written as

$$\tau_r = c_b(\dot{\phi}_r - \dot{\phi}_b) + k_b(\phi_r - \phi_b) - c_{rb}\dot{\phi}_b,$$

$\tau_s = \mu_{sb} R_b W_b$ is the static friction torque, μ_{sb} is the static friction coefficient, R_b is the bit radius, W_b is the WOB, $\xi > 0$ is a small constant, and

$$\mu_b = \mu_{cb} + (\mu_{sb} - \mu_{cb})\, e^{-\delta_b |\dot{\phi}_b|/v_f},$$

is a velocity-dependent friction coefficient following an exponentially decaying law. Here, μ_{cb} is the Coulomb friction coefficient, $0 < \delta_b < 1$ is a constant defining the velocity decreasing rate of T_b, v_f is a velocity constant.

2.2. Non-dimensional equations

Before carrying out the numerical study, we introduce the following non-dimensional variables:

$$\tau = \frac{c_p}{J_o} t, \ \theta_i = \phi_i, \ \theta_i' = \frac{J_o}{c_p}\dot{\phi}_i, \ \theta_i'' = \frac{J_o^2}{c_p^2}\ddot{\phi}_i, \ \upsilon = \frac{J_o}{c_p^2} u,$$

and parameters

$$\gamma_j = \frac{J_j}{J_o}, \ \beta_j = \frac{J_o}{c_p^2} k_j, \ \zeta_h = \frac{c_h}{c_p}, \ \eta = \frac{J_o}{c_p}\xi, \ \varepsilon = \frac{J_o R_b W_b}{c_p^2}, \ \lambda = \frac{J_o}{c_p} v_f,$$

where τ is the nondimensionalized time, $i = o, 1, 2, \ldots, n, r, b$, $j = p, r, b$, and $h = rt, r, b, rb$. In the expressions above, $\theta_i' = \frac{d\theta_i}{d\tau}$, $\dot{\phi}_i = \frac{d\phi_i}{dt}$ and so on. Hence, the generalized non-dimensional lumped-parameter model can be rewritten as

$$\bar{J}\Theta'' + \bar{C}\Theta' + \bar{K}\Theta + \bar{T} = \bar{U}, \tag{3}$$

where $\Theta = [\theta_o, \theta_1, \theta_2, \ldots, \theta_n, \theta_r, \theta_b]^T \in \mathbb{R}^{n+3}$ is a vector containing the angular positions of the discs, $\bar{J} = \text{diag}(1, \underbrace{\gamma_p, \gamma_p, \ldots, \gamma_p}_{n}, \gamma_r, \gamma_b) \in \mathbb{R}^{(n+3)\times(n+3)}$ is the inertia matrix, $\bar{C} \in \mathbb{R}^{(n+3)\times(n+3)}$ is the torsional damping matrix given by

$$\bar{C} = \begin{bmatrix} 1+\zeta_{rt} & -1 & 0 & 0 & \ldots & 0 & 0 & 0 & 0 \\ -1 & 2 & -1 & 0 & \ldots & 0 & 0 & 0 & 0 \\ 0 & -1 & 2 & -1 & \ldots & 0 & 0 & 0 & 0 \\ \ldots & \ldots & \ldots & \ldots & \ldots & \ldots & \ldots & \ldots & \ldots \\ 0 & 0 & 0 & 0 & \ldots & -1 & 1+\zeta_r & -\zeta_r & 0 \\ 0 & 0 & 0 & 0 & \ldots & 0 & -\zeta_r & \zeta_r+\zeta_b & -\zeta_b \\ 0 & 0 & 0 & 0 & \ldots & 0 & 0 & -\zeta_b & \zeta_b+\zeta_{rb} \end{bmatrix},$$

$\bar{K} \in \mathbb{R}^{(n+3)\times(n+3)}$ is the torsional stiffness matrix given by

$$\bar{K} = \begin{bmatrix} \beta_p & -\beta_p & 0 & 0 & \ldots & 0 & 0 & 0 & 0 \\ -\beta_p & 2\beta_p & -\beta_p & 0 & \ldots & 0 & 0 & 0 & 0 \\ 0 & -\beta_p & 2\beta_p & -\beta_p & \ldots & 0 & 0 & 0 & 0 \\ \ldots & \ldots & \ldots & \ldots & \ldots & \ldots & \ldots & \ldots & \ldots \\ 0 & 0 & 0 & 0 & \ldots & -\beta_p & \beta_p+\beta_r & -\beta_r & 0 \\ 0 & 0 & 0 & 0 & \ldots & 0 & -\beta_r & \beta_r+\beta_b & -\beta_b \\ 0 & 0 & 0 & 0 & \ldots & 0 & 0 & -\beta_b & \beta_b \end{bmatrix},$$

$\bar{T} = [0, 0, \ldots, \bar{T}_b]^T \in \mathbb{R}^{n+3}$, and $\bar{U} = [\upsilon, 0, \ldots, 0]^T \in \mathbb{R}^{n+3}$. Here, $\bar{T}_b$ can be rewritten as

$$\bar{T}_b = \begin{cases} \bar{\tau}_r = \zeta_b(\theta_r' - \theta_b') + \beta_b(\theta_r - \theta_b) - \zeta_{rb}\theta_b' & \text{if } |\theta_b'| < \eta \text{ and } |\bar{\tau}_r| \le \mu_{sb}\varepsilon, \\ \mu_{sb}\varepsilon \cdot \text{sgn}(\bar{\tau}_r) & \text{if } |\theta_b'| < \eta \text{ and } |\bar{\tau}_r| > \mu_{sb}\varepsilon, \\ \left[\mu_{cb} + (\mu_{sb} - \mu_{cb})\, e^{-\delta_b|\theta_b'|/\lambda}\right]\varepsilon \cdot \text{sgn}(\theta_b') & \text{if } |\theta_b'| \ge \eta. \end{cases} \tag{4}$$

3. Mathematical formulation of the drill-string system in COCO

In order to carry out a detailed investigation of the torsional stick-slip vibration and the multistability in the drill-string system shown in Fig. 2(b), we will apply numerical continuation methods for non-smooth dynamical systems, implemented via the continuation platform COCO [29]. The stick-slip vibrations that are studied in the present work can be characterized by two modes of operation, as specified below.

Slip (SL). In this mode, the drill-bit rotates with positive angular velocity, and the drill-string motion is governed by the equations

$$\begin{cases} \theta_o'' + \zeta_{rt}\theta_o' + (\theta_o' - \theta_1') + \beta_p(\theta_o - \theta_1) = \upsilon, \\ \gamma_p\,\theta_1'' + (\theta_1' - \theta_o') + (\theta_1' - \theta_2') + \beta_p(\theta_1 - \theta_o) + \beta_p(\theta_1 - \theta_2) = 0, \\ \ldots \\ \gamma_r\theta_r'' + \zeta_r(\theta_r' - \theta_n') + \zeta_b(\theta_r' - \theta_b') + \beta_r(\theta_r - \theta_n) + \beta_b(\theta_r - \theta_b) = 0, \\ \gamma_b\theta_b'' + \zeta_{rb}\theta_b' + \zeta_b(\theta_b' - \theta_r') + \beta_b(\theta_b - \theta_r) + T_b^{\text{SL}} = 0. \end{cases} \tag{5}$$

Here, the reaction torque is computed through the formula

$$T_b^{\text{SL}} = \begin{cases} T_0, & \theta_b' = 0, \\ \left[\mu_{cb} + (\mu_{sb} - \mu_{cb})e^{-\delta_b\theta_b'/\lambda}\right]\varepsilon, & \theta_b' > 0, \end{cases} \tag{6}$$

which is a simplified version of the torque function shown in Eq. (4). In the expression above, $T_0 = \mu_{sb}\varepsilon$ is the break-away torque, and this operation mode terminates at some $t = t_{\text{stick}} \ge 0$ when the angular speed of the drill-bit becomes zero, i.e. $\theta_b'(t_{\text{stick}}) = 0$. At this time, the system switches to the stick mode of operation defined below.

Stick (ST). During this regime the drill-bit is in stationary position, and the system motion is described by the equations

$$\begin{cases} \theta_o'' + \zeta_{rt}\theta_o' + (\theta_o' - \theta_1') + \beta_p(\theta_o - \theta_1) = \upsilon, \\ \gamma_p\theta_1'' + (\theta_1' - \theta_o') + (\theta_1' - \theta_2') + \beta_p(\theta_1 - \theta_o) + \beta_p(\theta_1 - \theta_2) = 0, \\ \ldots \\ \gamma_r\theta_r'' + \zeta_r(\theta_r' - \theta_n') + \zeta_b\theta_r' + \beta_r(\theta_r - \theta_n) + \beta_b(\theta_r - \theta_b) = 0, \\ \theta_b'' = 0, \quad \theta_b' = 0. \end{cases} \tag{7}$$

During this mode, the reaction torque is computed via Newton's third law as follows

$$T_b^{\text{ST}} = \zeta_b\theta_r' + \beta_b(\theta_r - \theta_b), \tag{8}$$

which means that the reaction torque adjusts itself to enforce the equilibrium with the external torque acting on the drill-bit. This mode terminates at some $t = t_{\text{slip}} \ge 0$ when $T_b^{\text{ST}}\big|_{t=t_{\text{slip}}} = T_0$. At this point, the reaction torque has reached the break-away torque value T_0, where the drill-bit begins to rotate, hence switching the system to the slip phase introduced previously.

Table 1
Nondimensional parameters of the drill-string system adopted from a real drill-string design [32].

Parameter	value	Parameter	value	Parameter	value
γ_p	3.08	ζ_{rb}	0.53	μ_{cb}	0.45
γ_r	0.82	β_p	28.31	μ_{sb}	0.8
γ_b	0.49	β_r	43.68	η	6×10^{-6}
ζ_r	1.27	β_b	36.80	ν_f	1
ζ_b	1.20	δ_b	0.85	υ	various
ζ_{rt}	2.73	λ	0.14	ε	various

In the following section, we will carry out numerical analysis using the drill-string model (5)–(8). The nondimensional parameters of the system, which were obtained from a real drill-string design [32], are given in Table 1.

4. Numerical analysis

Drill-string model can exhibit parameter regions for which multiple stable states coexist, for instance, bit-sticking equilibria, stick-slip vibrations, and the equilibria with constant rotation. These states are very sensitive to their initial conditions, and their coexistence under varying WOB have been preliminarily studied in [9]. We will study this multistability in this section further with consideration of the control torque and the length of drill-strings by using the path-following methods. Here, the results of the numerical investigation will be presented using the following solution measure

$$M_{\omega_b} = \frac{1}{T_0}\int_0^{T_0} \theta_b'(\tau)\,\mathrm{d}\tau, \tag{9}$$

which gives the average angular velocity of the drill-bit in the time window $[0, T_0]$, where T_0 is a suitably chosen positive number. In the case of studying periodic orbits, T_0 will correspond to the period of the solution.

4.1. Conditions for coexistence

Define a switching manifold

$$\Gamma := \{\Theta \in \Re^{n+3} : \ \theta_b' = 0\}$$

and an attractive region

$$\widetilde{\Gamma} := \{\Theta \in \Gamma : \ |\zeta_b\theta_r' + \beta_b(\theta_r - \theta_b)| < \mu_{sb}\varepsilon\}$$

which is a subset of Γ. According to the presence of friction at the bit-rock interface, if the control torque υ is a constant value, three stable states may coexist for the drill-string system which are studied as below.

Bit sticking: For any $\tau > \tau_{bs}$, $\Theta \in \widetilde{\Gamma}$, where τ_{bs} is the time that drill-string trajectory reaches $\widetilde{\Gamma}$ and stays in the region thereafter. If a new state of the drill-string system is defined as

$$x = [\theta_o',\ \theta_o - \theta_1,\ \theta_1',\ \theta_1 - \theta_2,\ \ldots,\ \theta_n',\theta_n - \theta_r,\ \theta_r',\ \theta_r - \theta_b,\ \theta_b']^T,$$

the region of bit sticking has an asymptotically stable equilibrium given by

$$x_{bs} = \left[0,\ \tfrac{\upsilon}{\beta_p},\ 0,\ \tfrac{\upsilon}{\beta_p},\ \ldots,\ 0,\ \tfrac{\upsilon}{\beta_p},\ 0,\ \tfrac{\upsilon}{\beta_r},\ 0,\ \tfrac{\upsilon}{\beta_b},\ 0\right]^T.$$

Fig. 3(a) presents a bit sticking motion of the drill-string showing the system has a stable equilibrium at $x_{bs} = [0,\ 4.57,\ 0,\ 2.96,\ 0,\ 3.52,\ 0]^T$. As can be seen from the lower plot of Fig. 3(a), the torque on bit increases initially when the drill-bit rotates. When $\tau = 0.28$, the drill-bit stops rotating and the torque on bit suddenly reduces due to the change of the frictional law (4). Then the torque on bit is built up again, however, its maximum cannot achieve the level of the break-away torque defined by the static friction torque $\mu_{sb}\varepsilon$. Hence, the trajectory of the drill-string reaches $\widetilde{\Gamma}$ and stays in this attractive region thereafter. Finally, the constant control torque υ equals to the torque on bit and all the other torques on the drill-string are balanced.

Stick-slip vibration: If the trajectory of the drill-string enters and leaves $\widetilde{\Gamma}$, the drill-bit is experiencing stick-slip vibrations. Fig. 3(b) shows an example of the stick-slip motion of the drill-string system using the same parameters in Table 1 but with a different set of initial conditions. It can be seen that at the beginning of the upper plot of Fig. 3(b), high quantities of friction are seen to cause the drill-bit (green line) to stall. Then, at about $\tau = 0.79$, the drill-bit becomes loose and rotate vigorously, up to a speed greater than that of the rotary table (black line). This is due to the fact that at $\tau = 0.79$, the torque on bit achieves the static friction torque $\mu_{sb}\varepsilon$ (dash line) as shown in the lower plot of Fig. 3(b). However, at about $\tau = 1.21$, the angular speed of the drill-bit decreases to the point at which is stalled again at $\tau = 1.54$. This motion repeats

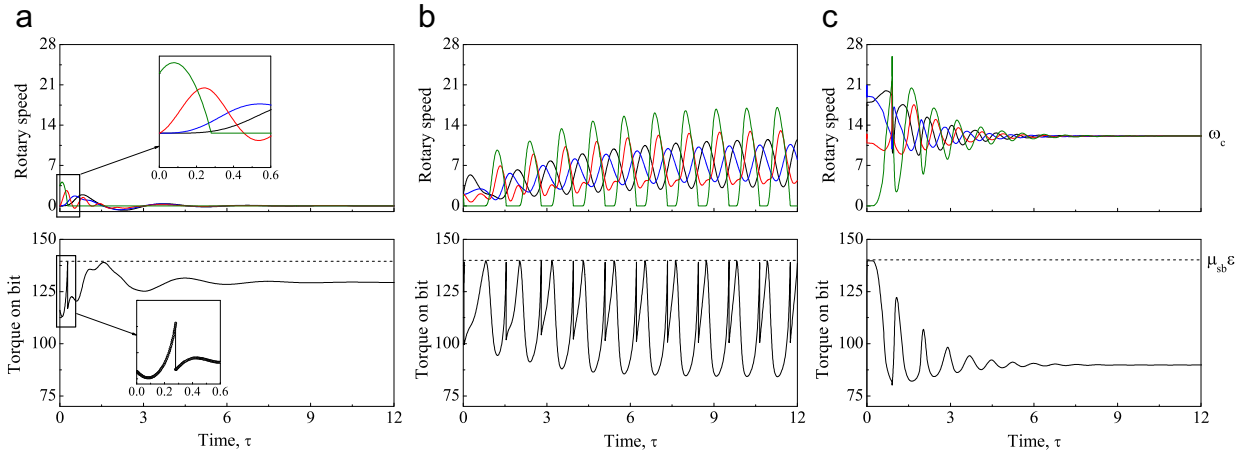

Fig. 3. (Colour online) Time responses of the angular speeds (upper) of the rotary table (black), drill pipe (blue), drill collar (red), and drill-bit (green), and torque on bit (lower) at where (a) bit sticking, (b) stick-slip vibrations, and (c) constant rotation coexist for $n = 1$, $\varepsilon = 174.72$, and $\upsilon = 129.42$. (For interpretation of the references to color in this figure legend, the reader is referred to the web version of this article.)

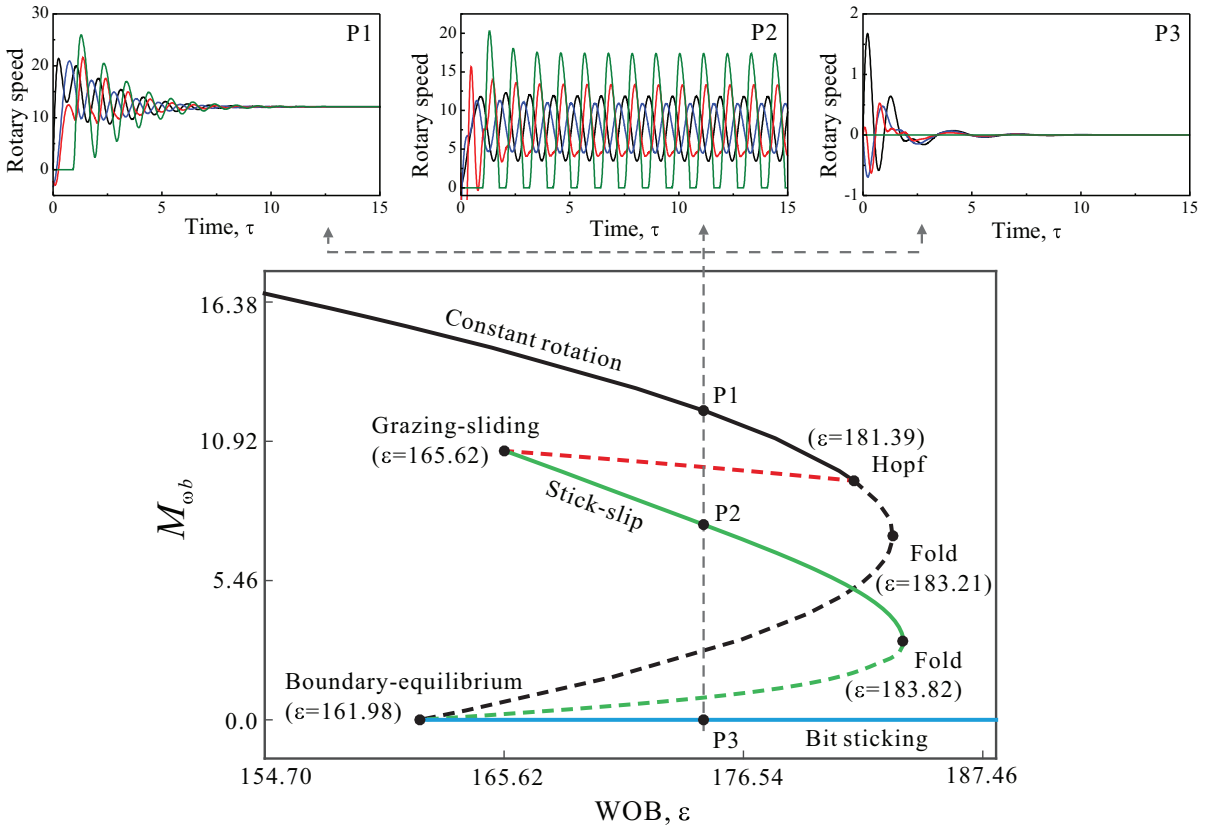

Fig. 4. (Colour online) Numerical continuation of the dynamical response of the drill-string system for $n = 1$ and $\upsilon = 129.42$ with respect to the WOB, ε. The black and blue curves represent the continuation of equilibrium points corresponding to constant rotation and bit sticking, respectively. Green curve stands for the continuation of stick-slip solutions, while the red branch corresponds to periodic solutions with no sticking phases. Solid and dashed lines denote stable and unstable solutions, respectively. Additional windows show the time responses of the angular velocities of the drill-bit (green), collar (red), pipe (blue), and rotary table (black) at $\varepsilon = 174.72$ for constant rotation (P1), stick-slip vibration (P2), and bit sticking (P3). (For interpretation of the references to color in this figure legend, the reader is referred to the web version of this article.)

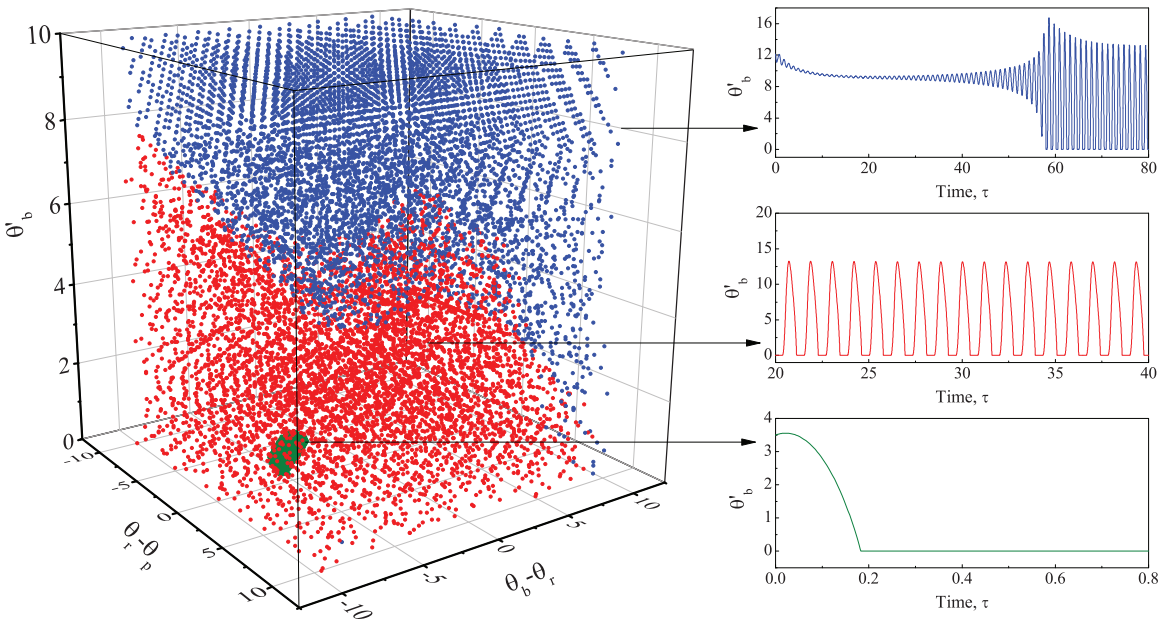

Fig. 5. (Colour online) Basins of attraction of the drill-string system calculated for $n = 1$, $\varepsilon = 182$, and $\upsilon = 129.42$ showing bistability where bit sticking (green dots) and stick-slip vibrations (red and blue dots) coexist. The original basin of constant rotation (blue dots) loses stability after the Hopf bifurcation at $\varepsilon = 181.39$ shown in Fig. 4. The right panels present the time responses of the angular velocity of the drill-bit. (For interpretation of the references to color in this figure legend, the reader is referred to the web version of this article.)

throughout the graph highlighting the cyclic nature of stick-slip vibrations. It is also important to note that during this phenomenon, torsional waves can be generated at the drill-bit and then travel back up along the drill-string to the surface. This can cause changes in the rotary table oscillations, which is detrimental to not only the part of the drilling rig but also can produce the bit bouncing and whirling phenomena.

Constant rotation: The bit can move at a positive constant rotary speed and its standard equilibrium is

$$x_c = \left[\omega_c,\ \frac{h}{\beta_p},\ \omega_c,\ \frac{h}{\beta_p},\ \ldots,\ \omega_c,\ \frac{h}{\beta_p},\ \omega_c,\ \frac{h}{\beta_r},\ \omega_c,\ \frac{h}{\beta_b},\ \omega_c\right]^T,$$

where ω_c is a constant value,

$$h = \frac{\zeta_{rt}\left[\mu_{cb} + (\mu_{sb} - \mu_{cb})\, e^{-\delta_b|\theta_b'|/\lambda}\right]\varepsilon \cdot \mathrm{sgn}(\omega_c) + \zeta_{rb}\upsilon}{\zeta_{rt} + \zeta_{rb}},$$

and

$$(\zeta_{rt} + \zeta_{rb})\,\omega_c + \left[\mu_{cb} + (\mu_{sb} - \mu_{cb})\, e^{-\delta_b|\omega_c|/\lambda}\right]\varepsilon \cdot \mathrm{sgn}(\omega_b) = \upsilon.$$

A coexisting constant rotation equilibrium of the drill-string system is shown in Fig. 3(c), where the drill-bit (green line in the upper plot) breaks away the static friction torque $\mu_{sb}\varepsilon$ (dash line in the lower plot) at the start of the simulation. Then the rotary speeds settle down to a constant value ω_c quickly and the drill-string system is stabilized at the equilibrium $x_c = [12.12,\ 3.4,\ 12.12,\ 2.2,\ 12.12,\ 2.62,\ 12.12]^T$. It is worth noting that this equilibrium is the desired state of drilling control, and many control methods (e.g. [8,27,30]) have been developed to suppress stick-slip vibration and bit sticking phenomena. However, due to the non-smooth nature of the friction at the bit-rock interface, complete suppression of these two phenomena are not possible. Therefore, a viable way of controlling drill-strings for constant rotation is to avoid such multistable area and operate the system at a monostable region, where only equilibria with constant rotation exist. Realization of this would need determination of the basins of attraction of the drill-string system, which is addressed later in the work.

4.2. Variation of WOB

The result of the numerical continuation of the dynamical response of the drill-string model (5–8) for $n = 1$ under variation of the WOB, ε, showing the average angular speed of the drill-bit, M_{ω_b}, on the vertical axis, is presented in Fig. 4, where stable and unstable solutions are represented by solid and dashed lines, respectively. The continuation was carried out starting from $\varepsilon = 154.70$, and in this case, all four disks rotate with a constant angular speed, which is represented by the system as a stable equilibrium denoted by a black curve in the figure. This equilibrium persists until $\varepsilon = 181.39$ when a subcritical Hopf bifurcation, which corresponds to the so-called catastrophic loss of stability, is encountered. An

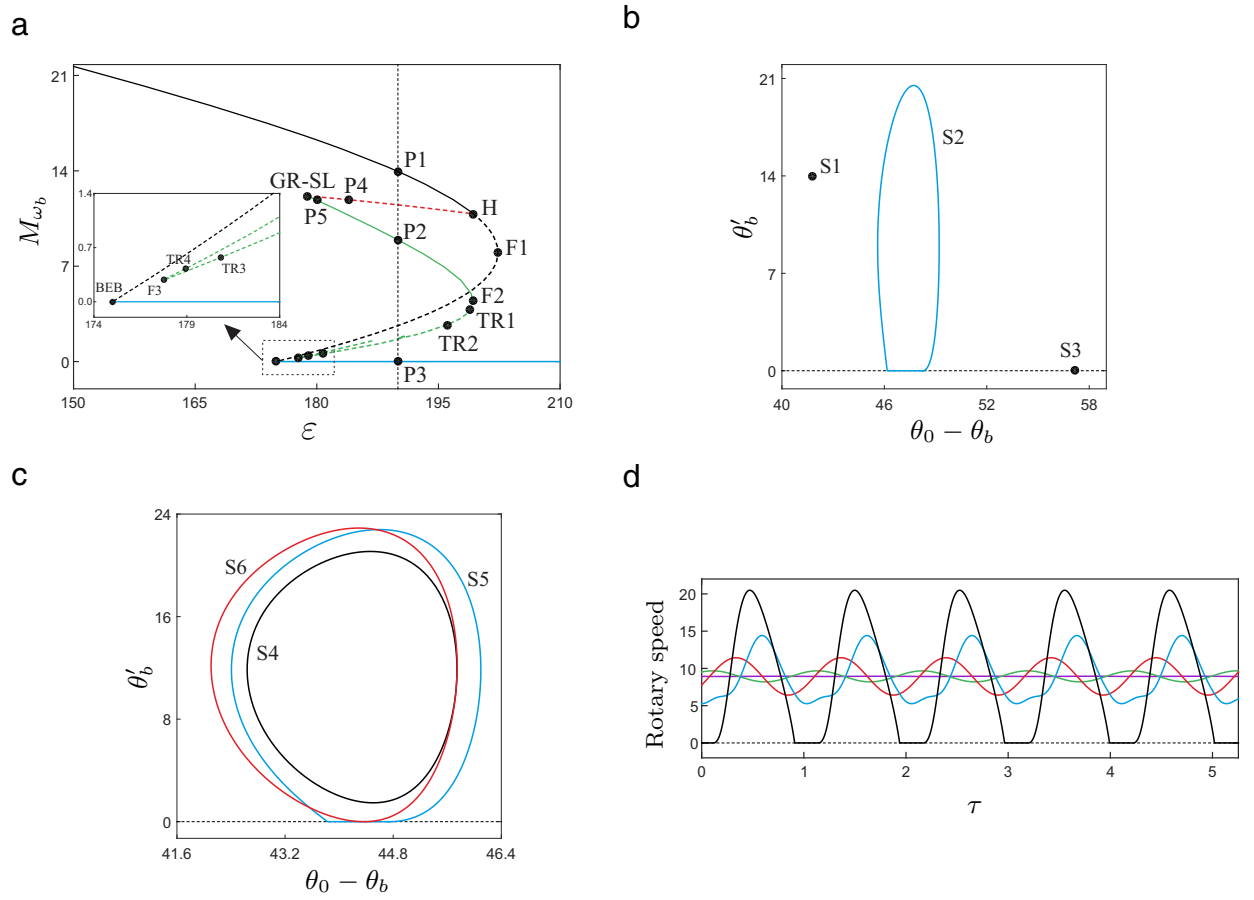

Fig. 6. (a) Numerical continuation of the dynamical response of the drill-string model with $n = 10$, i.e., 13 disks. The bifurcation picture is carried out with respect to ε, for the parameter values given in Table 1, with $\nu = 140$. The black and blue curves represent the continuation of equilibrium points corresponding to $\omega_b > 0$ (constant rotation) and $\omega_b = 0$ (permanent sticking), respectively. The green curve stands for the continuation of stick-slip solutions, while the red branch corresponds to periodic solutions with no sticking phases. Solid and dashed lines denote stable and unstable solutions, respectively. The vertical axis gives the average angular speed of the drill-bit, denoted by M_{ω_b}. (b) Phase portrait showing three coexisting attractors: S1 (equilibrium with $\omega_b > 0$), S2 (stick-slip solution) and S3 (equilibrium with $\omega_b = 0$) corresponding to the test points P1, P2 and P3, respectively, shown in panel (a) with $\varepsilon = 190$. Panel (c) presents three solutions labeled S4, S5 and S6 computed around the grazing-sliding bifurcation GR-SL, for P4 ($\varepsilon = 184$), P5 ($\varepsilon = 180$) and GR-SL ($\varepsilon \approx 178.85$), respectively. (d) Time response of the stick-slip solution S2 showing the angular speeds ω_b (black), ω_r (blue), ω_9 (red), ω_7 (green) and ω_0 (purple). (For interpretation of the references to color in this figure legend, the reader is referred to the web version of this article.)

unstable branch of equilibria shown by dashed black curve can be traced after the Hopf bifurcation until a fold bifurcation is detected at $\varepsilon = 183.21$. Then the unstable branch is traced toward the decreasing direction of the WOB and collides with a branch of stable equilibria marked by a solid blue curve through a boundary-equilibrium bifurcation at $\varepsilon = 161.98$. This blue curve, which persists for increasing WOB, represents the continuation of stable equilibrium for which the drill-bit permanently sticks at the borehole. At the boundary-equilibrium point $\varepsilon = 161.98$, a branch of unstable periodic orbits marked by dashed green line is detected. As the value of WOB increases, this branch collides with the branch of stable periodic orbits (solid green line) through a fold bifurcation of limit cycles at $\varepsilon = 183.82$. Both of the unstable and stable periodic orbits correspond to the stick-slip vibrations of the drill-strings. By tracing this stable stick-slip orbit, the collision with another branch of unstable periodic orbits (dashed red line) representing pure oscillations of the drill-strings, which is created by the subcritical Hopf bifurcation (at $\varepsilon = 181.39$), is found at $\varepsilon = 165.62$ via a grazing-sliding bifurcation.

An important observation from Fig. 4 is that the drill-string system exhibits three coexisting states for $\varepsilon \in [165.62, 181.39]$, and two for $\varepsilon \in [161.98, 165.62]$ and $\varepsilon \in [181.39, 183.82]$. For $\varepsilon < 161.98$ and $\varepsilon > 183.82$, the system is monostable, i.e. either rotating at a constant speed or permanently sticking at the borehole. Additional windows in Fig. 4 show the time responses of the angular velocity of the drill-string system in three coexisting states, constant rotation (P1), stick-slip vibration (P2), and bit sticking (P3). Fig. 5 demonstrates the change of these three coexisting states from losing the stability of constant rotation by presenting the basins of attraction of the system at $\varepsilon = 182$. It can be seen from the figure that bit sticking (green dots), stick-slip (red dots), and constant rotation (blue dots) coexist originally, but constant rotation becomes unstable (see the right panel) after the Hopf bifurcation. It also should be noted that most of the initial conditions in the figure converge

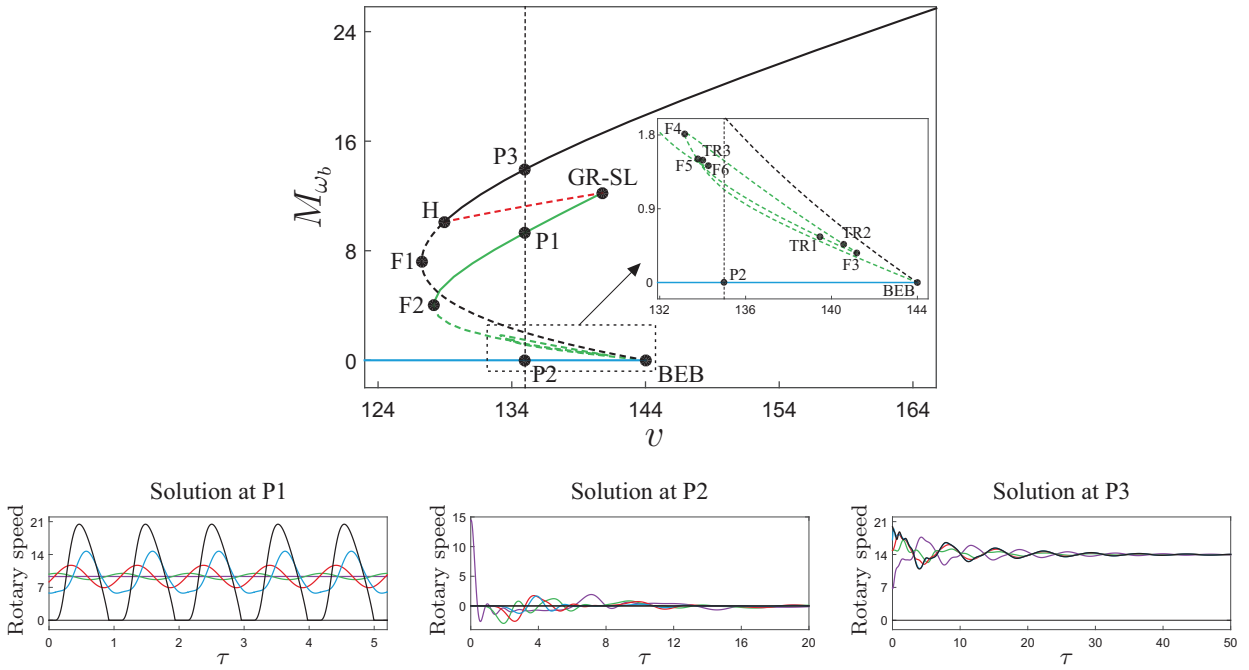

Fig. 7. Numerical continuation of the dynamical response of the drill-string model with $n = 10$, i.e., 13 disks. The bifurcation picture is carried out with respect to v, for the parameter values given in Table 1, with $\varepsilon = 180$. The black and blue curves represent the continuation of equilibrium points corresponding to $\omega_b > 0$ (constant rotation) and $\omega_b = 0$ (permanent sticking), respectively. The green curve stands for the continuation of stick-slip solutions, while the red branch corresponds to periodic solutions with no sticking phases. Solid and dashed lines denote stable and unstable solutions, respectively. The vertical axis gives the average angular speed of the drill-bit, denoted by M_{ω_b}. The lower panels depict three coexisting stable solutions computed for $v = 135$, showing the coexistence of constant rotation, permanent sticking and stick-slip phenomena for the same set of parameter values. The time plots show the angular speeds ω_b (black), ω_r (blue), ω_9 (red), ω_7 (green) and ω_0 (purple). (For interpretation of the references to color in this figure legend, the reader is referred to the web version of this article.)

to stick-slip vibrations. So, in the bistable region $\varepsilon \in [181.39, 183.82]$, stick-slip vibrations still dominate the system. However, after the fold bifurcation at $\varepsilon = 183.82$, such vibrations disappear, and the drill-string system becomes monostable exhibiting permanently sticking only.

4.3. Variation of drill-string length

Another question that we tackle in our numerical study is whether the bifurcation picture changes significantly when a higher number of disks is considered. Practically speaking, this situation amounts to drilling deeper, which is a scenario that should be considered as well. This case is analyzed in Fig. 6, which is obtained by choosing $n = 10$, i.e., considering 13 disks in the physical model depicted in Fig. 2(b). In general terms, the resulting bifurcation picture is very close to the one shown in Fig. 4, which was computed for $n = 1$. One of the main differences is the appearance of torus bifurcation of limit cycles, which are detected at $\varepsilon \approx 198.87$ (TR1), $\varepsilon \approx 196.07$ (TR2), $\varepsilon \approx 180.83$ (TR3) and $\varepsilon \approx 178.94$ (TR4). These bifurcations, however, occur for unstable periodic orbits, due to which they do not affect the system behaviour because the emerging quasiperiodic solutions are unstable. The remaining bifurcation points are of the same type as before, detected at $\varepsilon \approx 199.32$ (H, Hopf), $\varepsilon \approx 202.34$ (F1, fold) and $\varepsilon = 175$ (BEB, boundary-equilibrium bifurcation), which are all bifurcation of equilibria. Bifurcations of limit cycles occur for $\varepsilon \approx 178.85$ (GR-SL, grazing-sliding), $\varepsilon \approx 199.25$ (F2, fold) and $\varepsilon \approx 177.78$ (F3, fold). Similarly as before, the bifurcation picture reveals the presence of a parameter window in which multistability is observed. This window is limited by the fold (F2) and the grazing-sliding bifurcation detected during the analysis.

4.4. Variation of control torque

Numerical continuation of the dynamical response of the drill-string model with $n = 10$ (i.e. 13 disks) under variation of control torque, υ is presented in Fig. 7, where solid and dashed lines denote stable and unstable solutions, respectively. Generally speaking, the resulting bifurcation picture is very close to the ones obtained by varying the value of WOB, which were computed for $n = 1$ and $n = 10$. In this figure, black and blue curves represent the continuation of equilibrium points corresponding to constant rotation ($\omega_b > 0$) and bit sticking ($\omega_b = 0$), respectively. The stable equilibria for constant rotation exist for $\upsilon > 128.95$, and the angular velocity of the drill-bit increases as the control torque υ increases. At $\upsilon = 128.95$, a Hopf bifurcation is detected, and a branch of unstable equilibria marked by dashed black line can be traced toward the

decreasing direction of the control torque. Then, this unstable branch makes a "u-turn" through a fold bifurcation (F1) at $\upsilon = 127.25$ and collides with the stable equilibria of bit sticking (blue curve) via a boundary-equilibrium bifurcation at $\upsilon = 144$. The branch of stable periodic solutions denoted by solid green curve representing the stick-slip vibrations is found to exist between a fold bifurcation (F2) and a grazing-sliding bifurcation for $\upsilon \in (128.15,\ 140.78)$. The branch of unstable periodic orbits denoted by dashed red curve representing pure oscillations of the drill-strings is recorded between the subcritical Hopf bifurcation and the grazing-sliding bifurcation. The remaining bifurcation points of limit cycles are $\upsilon \approx 139.48$ (TR1), $\upsilon \approx 140.56$ (TR2), $\upsilon \approx 134.01$ (TR3), $\upsilon \approx 141.17$ (F3), $\upsilon \approx 133.15$ (F4), $\upsilon \approx 133.78$ (F5), and $\upsilon \approx 134.26$ (F6). However, these bifurcations occur for unstable periodic orbits, so they do not affect the behaviour of the drill-string system.

4.5. Region of multistability

In order to obtain an insight into the multistability of the drill-string system, a two-parameter continuation of the Hopf (blue line), grazing-sliding (red line), fold (black line), and boundary-equilibrium (green line) bifurcations found in Fig. 6 was performed in Fig. 8 under the variations of the WOB and the control torque. It can be seen from Fig. 8(a) that, these curves define two regions of multistability, where solutions with constant rotation and permanent sticking coexist in the yellow area, and constant rotation, permanent sticking, and stick-slip coexist in the grey area. The areas above and below these multistable regions showing monostability of the system yield solutions with constant rotation and permanent sticking, respectively. Fig. 8(b) demonstrates three coexisting solutions computed for each of the test points P1 ($\varepsilon = 235,\ \nu = 168$), P2 ($\varepsilon = 300,\ \nu = 215$), and P3 ($\varepsilon = 368,\ \nu = 246$). In practice, the drill-string system should be operated in the monostable region where only constant rotation exists. The location of the boundary-equilibrium bifurcation curve (green line) shown in Fig. 8(a) will change when drilling becomes deeper leading the drill-string system to enter the bistable region marked by yellow. In this region, the system may exhibit either constant rotation or bit sticking which needs to be avoided. Therefore, a control strategy that can prevent the occurrence of this boundary-equilibrium bifurcation would be desirable.

5. Conclusions

This paper studied the torsional stick-slip vibrations of drill-strings using a generalized lumped-parameter model focusing on its multistable characteristics, i.e., the coexistence of bit sticking, stick-slip vibrations, and constant rotation. Our mathematical model was based on the lumped-parameter model [30], which includes a rotary table, a drill pipe, a drill collar, and a drill-bit. The main concern in our study was the undesired torsional vibrations and the coexistence of multiple stable states, whose analysis was carried out via path-following methods implemented through the continuation platform COCO [29].

Numerical analysis of coexisting states of the drill-string system under a constant control torque was carried out. The conditions of bit sticking, stick-slip, and constant rotation were given, and the existence of their multistable states was discussed. It was found that the attractive region $\widetilde{\Gamma}$ defined in Section 4.1 plays a significant role for the existence of multiple stable states in the drill-string model. If the trajectory of the drill-string system reaches $\widetilde{\Gamma}$ and stays in the region thereafter, the drill-bit will be stuck in borehole. If the trajectory enters and leaves $\widetilde{\Gamma}$ repetitively, the drill-bit exhibits stick-slip vibrations. If the trajectory enters and leaves $\widetilde{\Gamma}$ thereafter, the drill-bit will move at a constant rotary speed.

In order to investigate the influence of drilling depth on stick-slip vibrations, we compared the numerical continuations of coexisting states for the drill-strings with one pipe ($n = 1$) and ten pipes ($n = 10$). In general terms, the resulting bifurcation diagram for $n = 10$ is very close to the one computed for $n = 1$. One of the main differences is the appearance of torus bifurcation of limit cycles. However, these bifurcations occur for unstable periodic orbits which do not affect the behaviour of the drill-string system from a practical point of view. It is also worth noting that both stick-slip vibrations and multistability exist for a larger window of WOB when drilling becomes deeper.

Numerical continuation of the dynamical response of the drill-string model with $n = 10$ under the variation of the control torque was carried out. It was found that similar bifurcation structure as the ones for $n = 1$ and $n = 10$ under the variation of the WOB was recorded. The drill-string system with constant rotation may lose stability via a subcritical Hopf bifurcation, and the equilibrium of bit sticking will exist until a boundary-equilibrium bifurcation is encountered. Again, stick-slip vibrations exist between a fold bifurcation and a grazing-sliding bifurcation. In order to gain an insight into the multistability of the system, a two-parameter continuation of these bifurcations, i.e. the Hopf, grazing-sliding, fold, and boundary-equilibrium bifurcations, was performed under the variations of the WOB and the control torque. Two regions of multistability were identified, where solutions with constant rotation and bit sticking coexist, and constant rotation, bit sticking, and stick-slip coexist. In practice, the drill-string system should be operated in the monostable region where only constant rotation exists. As drilling becomes deeper, the boundary-equilibrium bifurcation curve which defines the boundary of monostability and bistability will change. Thus, a control strategy for the drill-string system preventing the occurrence of such bifurcation would be desirable.

Declaration of competing interest

The authors declare that they have no conflict of interest concerning the publication of this manuscript.

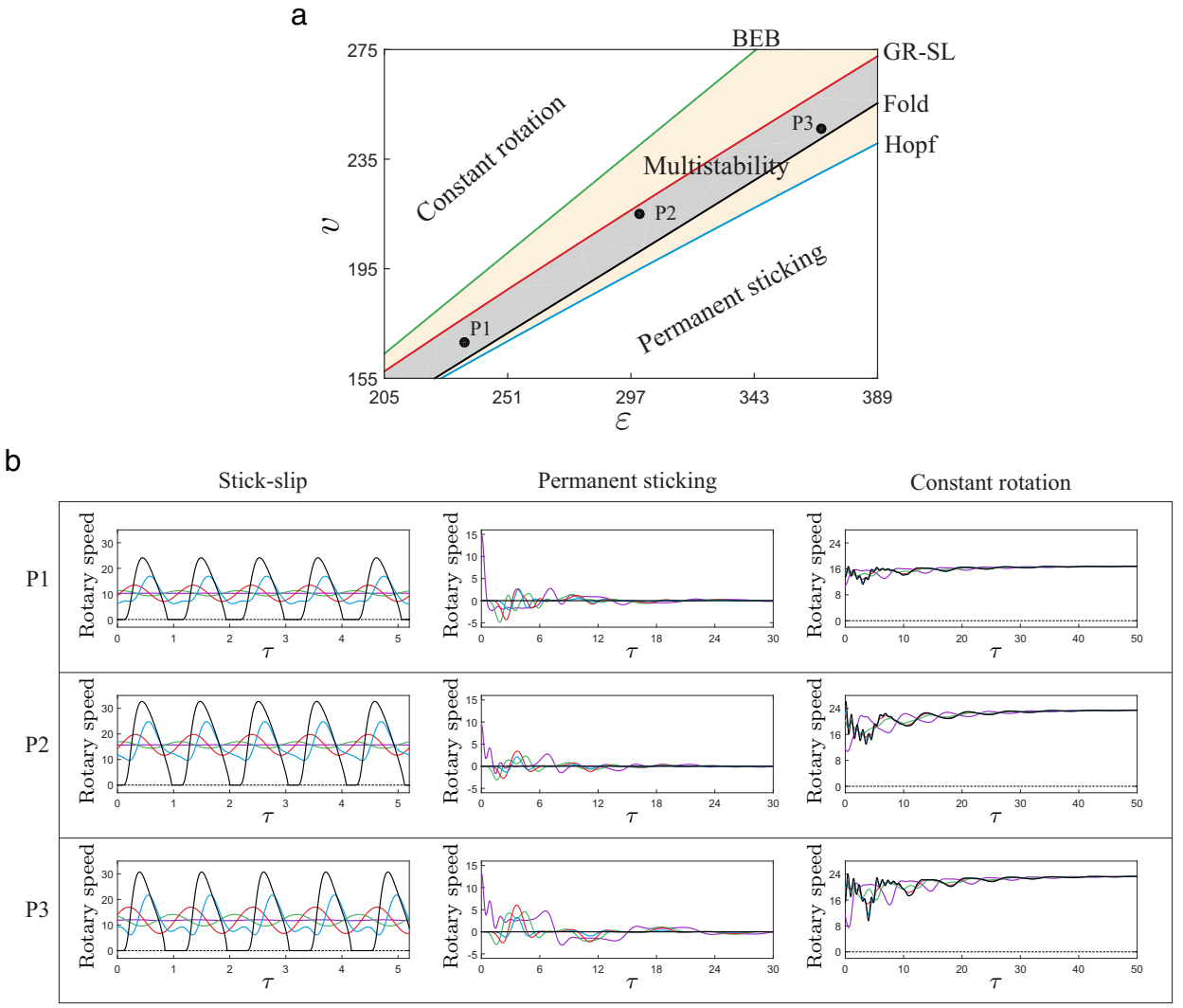

Fig. 8. (a) Two-parameter continuation of the Hopf (blue curve), grazing-sliding (red curve), fold (of limit cycles, black curve) and boundary-equilibrium (green curve) bifurcations found in Fig. 6(a), with respect to the WOB ε and the control torque υ. These curves define two regions of multistability, where solutions with constant rotation and permanent sticking coexist (yellow area), and constant rotation, permanent sticking and stick-slip coexist (grey area). The areas above and below these regions yield solutions with constant rotation and permanent sticking, respectively. Panel (b) shows three coexisting solutions computed for each of the test points P1 ($\varepsilon = 235,\ \upsilon = 168$), P2 ($\varepsilon = 300,\ \upsilon = 215$) and P3 ($\varepsilon = 368,\ \upsilon = 246$). The time responses show the angular speeds ω_b (black), ω_r (blue), ω_9 (red), ω_7 (green) and ω_0 (purple). (For interpretation of the references to color in this figure legend, the reader is referred to the web version of this article.)

Data accessibility

The datasets generated and analysed during the current study are available from the corresponding author on reasonable request.

Acknowledgements

This work has been supported by EPSRC under Grant No. EP/P023983/1. Dr Yang Liu would like to acknowledge the financial support from the National Natural Science Foundation of China (Grant Nos. 11672257 and 11872147). Mr Wei Lin would like to acknowledge the financial support from the China Scholarship Council (Award No. 201708510133) for his one year visiting study at the University of Exeter.

References

[1] E.M. Navarro-López, Bit-sticking phenomena in a multi-degree-of-freedom controlled drillstring, Explor. Prod. Oil Gas Rev. 8 (2010) 70–75.

[2] E. Detournay, P. Defourny, A phenomenological model for the drilling action of drag bits, Int. J. Rock Mech. Min. Sci. 29 (1) (1992) 13–23.
[3] E.M. Navarro-López, An alternative characterization of bit-sticking phenomena in a multi-degree-of-freedom controlled drillstring, Nonlinear Anal. Real World Appl. 10 (5) (2009) 3162–3174.
[4] P. Patil, C. Teodoriu, A comparative review of modelling and controlling torsional vibrations and experimentation using laboratory setups, J. Pet. Sci. Eng. 112 (2013) 227–238.
[5] Y. Kovalyshen, A simple model of bit whirl for deep drilling applications, J. Sound Vib. 332 (2013) 6321–6334.
[6] G.A. Leonov, N.V. Kuznetsov, M.A. Kiseleva, E.P. Solovyeva, A.M. Zaretskiy, Hidden oscillations in mathematical model of drilling system actuated by induction motor with a wound rotor, Nonlinear Dyn. 77 (1–2) (2014) 277–288.
[7] M. Kapitaniak, V. Vaziri Hamaneh, J. Páez Chávez, K. Nandakumar, M. Wiercigroch, Unveiling complexity of drill-string vibrations: experiments and modelling, Int. J. of Mech. Sci. 101–102 (2015) 324–337.
[8] T. Vromen, N. van de Wouw, A. Doris, P. Astrid, H. Nijmeijer, Nonlinear output-feedback control of torsional vibrations in drilling systems, Int. J. Robust Nonlinear Control 27 (2017) 3659–3684.
[9] Y. Liu, J. Páez Chávez, R. De Sa, S. Walker, Numerical and experimental studies of stick-slip oscillations in drill-strings, Nonlinear Dyn. 90 (2017) 2959–2978.
[10] M. Kapitaniak, V. Vaziri Hamaneh, J. Páez Chávez, M. Wiercigroch, Numerical study of forward and backward whirling of drill-string, J. Comput. Nonlin. Dyn. 12 (2017) 061009.
[11] M. Kapitaniak, V. Vaziri Hamaneh, J. Páez Chávez, M. Wiercigroch, Experimental studies of forward and backward whirls of drill-string, Mech. Syst. Signal Process. 100 (2018) 454–465.
[12] X. Liu, N. Vlajic, X. Long, G. Meng, B. Balachandran, Nonlinear motions of a flexible rotor with a drill bit: stick-slip and delay effects, Nonlinear Dyn. 72 (2013) 61–77.
[13] X. Liu, N. Vlajic, X. Long, G. Meng, B. Balachandran, State-dependent delay influenced drill-string oscillations and stability analysis, J. Vibr. Acoust. 136 (5) (2014) 051008.
[14] X. Liu, N. Vlajic, X. Long, G. Meng, B. Balachandran, Coupled axial-torsional dynamics in rotary drilling with state-dependent delay: stability and control, Nonlinear Dyn. 78 (3) (2014) 1891–1906.
[15] Y. Yan, M. Wiercigroch, Dynamics of rotary drilling with non-uniformly distributed blades, Int. J. Mech. Sci.. in press, doi:10.1016/j.ijmecsci.2019.05.016.
[16] J. Brett, The genesis of bit-induced torsional drillstring vibrations, SPE Drill. Eng. 7 (1992) 168–174.
[17] J.D. Jansen, L. van den Steen, Active damping of self-excited torsional vibrations in oil well drillstrings, J. Sound Vib. 179 (4) (1995) 647–668.
[18] S. Naganawa, Experimental analysis on vibrations of roller bit forces and motions, J. Jpn. Assoc. Pet. Technol. 62 (1997) 203–214.
[19] N. Mihajlović, A. van Veggel, N. van de Wouw, H. Nijmeijer, Analysis of friction-induced limit cycling in an experimental drill-string system, J. Dyn. Syst. Measur. Control 126 (2004) 709–720.
[20] R.I. Leine, D.H. van Campen, W.J.G. Keultjes, Stick-slip whirl interaction in drillstring dynamics, J. Vibr. Acoust. 124 (2) (2002) 209–220.
[21] H. Melakhessou, A. Berlioz, G. Ferraris, A nonlinear well-drillstring interaction model, J. Vib. Acoust. 125 (1) (2003) 46–52.
[22] C.M. Liao, B. Balachandran, M. Karkoub, Y.L. Abdel-Magid, Drill-string dynamics: reduced-order models and experimental studies, J. Vib. Acoust. 133 (4) (2011) 041008.
[23] V. Dunayevsky, F. Abbassian, Application of stability approach to bit dynamics, SPE Drill. Complet. 13 (1998).
[24] J. Kamel, A. Yigit, Modeling and analysis of stick-slip and bit bounce in oil well drillstrings equipped with drag bits, J. Sound Vib. 333 (2014) 6885–6899.
[25] L. Tang, X. Zhu, C. Shi, J. Tang, D. Xu, Study of the influences of rotary table speed on stick-slip vibration of the drilling system, Petroleum 1 (2015) 382–387.
[26] L. Hong, I. Girsang, J. Dhupia, Identification and control of stick-slip vibrations using Kalman estimator in oil-well drill strings, J. Pet. Sci. Eng. 140 (2016) 119–127.
[27] Y. Liu, Suppressing stick-slip oscillations in underactuated multibody drill-strings with parametric uncertainties using sliding-mode control, IET Control Theory Appl. 9 (2015) 91–102.
[28] B. Besselink, T. Vromen, N. Kremers, N. van de Wouw, Analysis and control of stick-slip oscillations in drilling systems, IEEE Trans. Control Syst. Tech. 24 (2016) 1582–1593.
[29] H. Dankowicz, F. Schilder, Recipes for continuation, in: Computational Science and Engineering, SIAM, Philadelphia, 2013.
[30] E.M. Navarro-López, E. Licéaga-Castro, Non-desired transitions and sliding-mode control of a multi-DOF mechanical system with stick-slip oscillations, Chaos Solit. Fract. 41 (4) (2009) 2035–2044.
[31] E.M. Navarro-López, D. Cortés, Avoiding harmful oscillations in a drillstring through dynamical analysis, J. Sound Vib. 307 (2007) 152–171.
[32] Tri-Cone Manual de Barrenas, Hughes Tool Company, USA, 1982.